Earth and Planetary Science Letters 270 (2008) 180–188

Contents lists available at ScienceDirect

Earth and Planetary Science Letters

journal homepage: www.elsevier.com/locate/epsl

Cyclic magma storages and transfers at Piton de La Fournaise volcano (La Réunion hotspot) inferred from deformation and geochemical data

Aline Peltier [a,b,*], Vincent Famin [a], Patrick Bachèlery [a], Valérie Cayol [c], Yo Fukushima [d], Thomas Staudacher [b]

[a] Laboratoire GéoSciences Réunion, Université de La Réunion, Institut de Physique du Globe de Paris, CNRS, UMR 7154, 15 avenue René Cassin, BP 7151, 97715 Saint Denis cedex 9, La Réunion, France
[b] Observatoire Volcanologique du Piton de la Fournaise, Institut de Physique du Globe de Paris, CNRS, UMR 7154, La Plaine des Cafres, La Réunion, France
[c] Laboratoire Magmas et Volcans, Université Blaise Pascal, CNRS, UMR 6524, Clermont-Ferrand, France
[d] Research Center for Earthquake Prediction, Disaster Prevention research Institute, Kyoto University, Kyoto, Japan

ARTICLE INFO

Article history:
Received 20 July 2007
Received in revised form 19 February 2008
Accepted 29 February 2008
Available online 13 March 2008

Edited by: C.P. Jaupart

Keywords:
Piton de La Fournaise
volcano activity
dyke injection
GPS
numerical modeling

ABSTRACT

Piton de La Fournaise is in a period of intense volcanic activity since 1998. To constrain the magma dynamics responsible for this activity, we combined GPS ground deformation monitoring interpreted through numerical modelling and geochemistry. Two cycles of continuous volcano inflation are evidenced for the May 2004–December 2005 period, with a rest from March to October 2005. These inflations are consistent with two cycles of compatible major element enrichment in the emitted lavas. Numerical models indicate that the pressurization of a single magma reservoir may be responsible for the observed pre-eruptive inflations of the volcano. The reservoir, located at 2300 m depth, has a radius of ~500 m. At the beginning of each cycle, dykes propagate from the roof of the reservoir and yield eruptions of differentiated basalt near the summit. At the end of the cycle, dykes propagate from the eastern sidewall of the reservoir and yield distal eruptions of primitive magmas away from the summit. The volumes of magma emitted during the primitive eruptions seem too large to explain the surface deformations and therefore suggest some refill of the reservoir by deeper magmas. Our results may be used to predict the location and lava volume of future eruptions at Piton de La Fournaise volcano, depending on the timing of these eruptions within a cycle of volcanic activity.

1. Introduction

An important issue in volcanology is to determine where magmas are stored beneath volcanoes, and how the different storage levels interact prior to and during eruptions. The study of these mechanisms is essential for a better understanding of volcano dynamics, and hence for the prediction of eruptions. Piton de La Fournaise volcano (La Réunion hotspot, Indian Ocean, Fig. 1a) is one of the best targets for the study of magma transfers because it is in a period of intense activity since 1998. The volcano is equipped with a large amount of monitoring networks, providing a continuous record of geophysical and geochemical data over the 1998–2006 period. At least three magma storage zones have been proposed at Piton de La Fournaise (PdF): 1) An array of sills and dykes slowly cooling at 0.5–1.5 km beneath the summit Dolomieu crater, as suggested by seismic and deformation features of the volcano during the 1980–1990 period (Bachèlery and Mairine, 1990); 2) a shallow reservoir at about 2.5 km depth evidenced by tomography and deformation data from the 1998–2006 period (Nercessian et al., 1996; Peltier et al., 2007); 3) a deeper storage zone at 7.5 km depth or more evidenced by the migration of earthquakes during the 1998 eruption (Battaglia et al., 2005). How and when these different storage zones are fed since 1998 remains completely unknown. In particular, whether the shallow and deeper reservoirs are continuously connected, transiently connected, or completely independent during a cycle of activity is a matter of debate. The aim of this paper is to constrain how magma is supplied to the different reservoirs prior to or during eruptions. The originality of our approach is to investigate the pattern of magma transport through a combination of ground deformation interpreted through numerical modelling and geochemical analyses. We focus on the exceptional dataset provided by the eruptions of May 2004, August 2004, February 2005, October 2005, November 2005 and December 2005. October 2005 eruption occurred in the summit crater (summit eruptions), May 2004, August 2004, and November 2005 eruptions on the slopes and/or at the base of the summit cone (proximal eruptions), and

* Corresponding author. Laboratoire GéoSciences Réunion, Université de La Réunion, Institut de Physique du Globe de Paris, CNRS, UMR 7154, 15 avenue René Cassin, BP 7151, 97715 Saint Denis cedex 9, La Réunion, France. Tel.: +33 262 0 2 62 93 82 05; fax: +33 262 0 2 62 93 82 66.
E-mail addresses: peltier@univ-reunion.fr (A. Peltier), Vincent.Famin@univ-reunion.fr (V. Famin), Patrick.Bachelery@univ-reunion.fr (P. Bachèlery), V.Cayol@opgc.univ-bpclermont.fr (V. Cayol), yofukushima@rcep.dpri.kyoto-u.ac.jp (Y. Fukushima), Thomas.Staudacher@univ-reunion.fr (T. Staudacher).

0012-821X/$ – see front matter © 2008 Elsevier B.V. All rights reserved.
doi:10.1016/j.epsl.2008.02.042

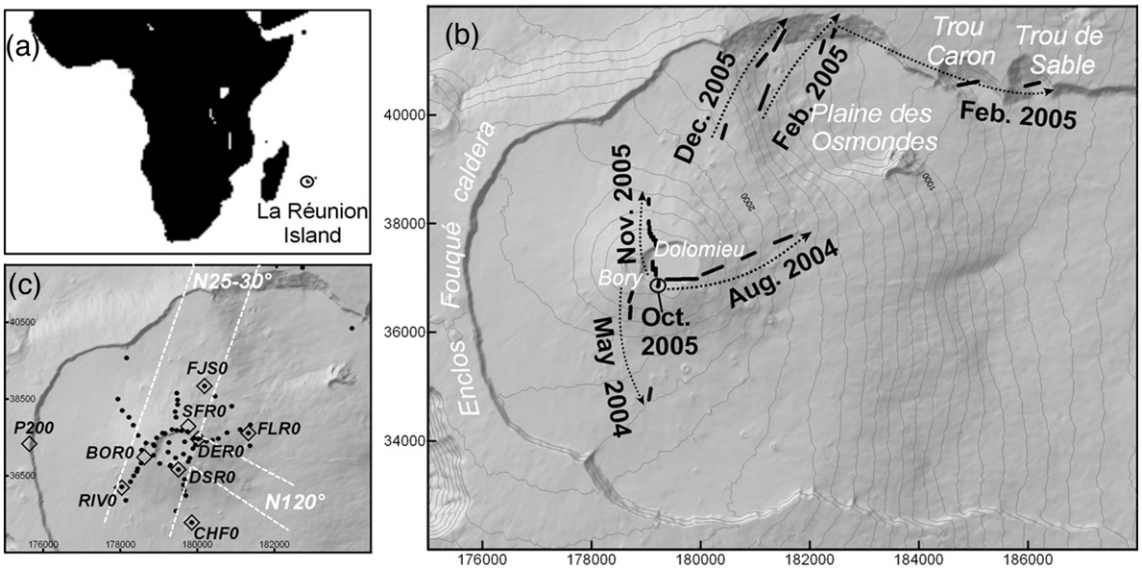

Fig. 1. (a) Localization of La Réunion Island. (b) Location of the 2004–2005 eruptive fissures on Piton de La Fournaise (Gauss Laborde Réunion coordinates). (c) Location of rift zones (white line, after Michon et al., 2007), permanent GPS stations (diamonds) and reiterated benchmark GPS measurements (dots).

February 2005 and December 2005 eruptions outside of the summit cone, more than 3 km away from the summit (distal eruptions) (Table 1, Fig. 1b).

2. Methods

2.1. Deformation data acquisition

Ground deformation of the volcanic edifice were monitored by the global positioning system (GPS) network of the Volcanological Observatory of Piton de La Fournaise (Fig. 1c). This network, initially composed of three summit stations (BOR0, SFR0, DSR0) and one reference station (P200), was implemented in August 2005 by four stations at the base of the volcano (FJS0, FLR0, CHF0, RIV0) and one at the summit (DER0). Each GPS station is composed of ASHTECH ZEXTREM, TRIMBLE NETRS or TOPCON GB-1000 apparatus installed on a stainless steel rod cemented in the bedrock or on concrete pillars. Data are acquired at 30 s intervals. The position of each station is calculated relatively to the reference station using the WINPRISM software. In addition to the permanent GPS network, the position of 80 stainless steel benchmarks (Fig. 1c) was measured immediately after each eruption with an acquisition time of 7 min at a period of 1 measurement per second.

2.2. Numerical modelling

Modelling is applied to constrain the depth, shape and overpressure of magma bodies that can account for the observed deformations

Table 1
Summary of quantitative data for the 2004–2005 eruptions

	Date of eruption	May 2nd–18th 2004	Aug. 13th–Oct. 16th 2004	Feb. 17th–26th 2005	Oct. 4th–17th 2005	Nov. 29th 2005	Dec. 26th, 2005–Jan. 17th, 2006
Field data	Eruption duration (days)	16	64	8	14	1	23
	Elevation (highest and lowest point) (m)	2525–2000	2540–1900	1650–500	2490	2490–2350	2025–1600
	Distance from the summit (m)	820–2545	0–2320	3270–5340	0	0–1270	2520–4870
	Pre-eruptive inflation duration (days)	74	48	87	125	42	25
	Seismic crisis duration (min)	31	25	170	54	25	130
	Vertical injection duration (min)[a]	13	14	28	25	12	7
	Lateral injection duration (min)[b]	6	8	142	31	18	130
	Post-eruptive deflation duration (days)	–	–	95	–	–	68
	Emitted volume (10^6 m^3)	16.4	20	20	2	1	~20
Dyke models	Volume (10^6 m^3)	1.2	0.7	3.8	0.39	0.68	5.2
	ΔP (MPa)	2.2	1.1	2	2.2	2.1	1.7
	Consistency (%)[c]	89	77	65	86	81	75
Pre-eruptive inflation source models	ΔP (MPa)	No data	4.7	3.4	4.3	5.2	3.7
	ΔV (10^6 m^3)	No data	0.58	0.41	0.55	0.65	0.44
	Consistency (%)[c]	No data	89	79	71	77	84
Post-eruptive deflation source models	ΔP (MPa)	–	–	−5.37	–	–	−0.8
	ΔV (10^6 m^3)	–	–	−0.66	–	–	−0.2 (dyke −0.8)
	Consistency (%)[c]	–	–	93	–	–	76

[a]Taken as the time lapse between the beginning of the summit inflation and the beginning of the lateral displacement of the inflation centre (Peltier et al., 2005).
[b]Taken as the time lapse between the beginning of the lateral displacement of the inflation centre and the opening of the first eruptive fissure.
[c]Defined as 100% minus the misfit between displacement data and the model.

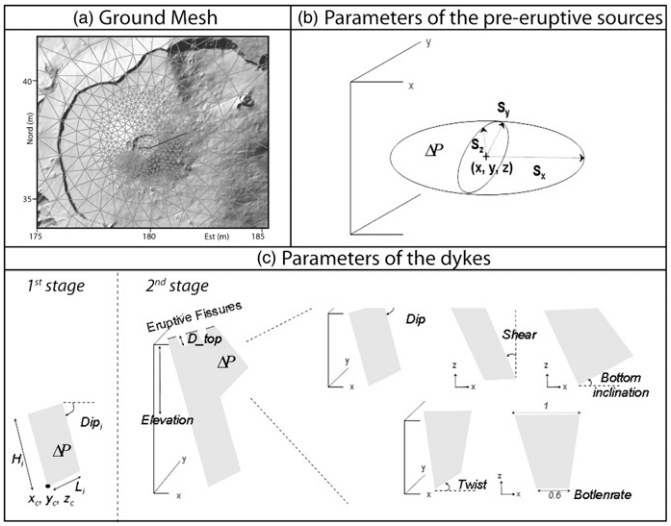

Fig. 2. Structures used in the modelling (a) Ground mesh (detail) on the example of the August 2004 dyke injection (b, c) Parameters used to model pre-eruptive sources of pressure and dyke injections, respectively.

at the surface of the volcano. Recorded GPS data are therefore used as an input in a three dimension (3D) elastic model based on a mixed boundary element method (MBEM) (Cayol and Cornet, 1997). The model is combined with Sambridge's Monte Carlo inversion method (Sambridge, 1999a) to minimize the misfit function (Fukushima et al., 2005), i.e. the normalized root mean square error between calculated and observed displacements.

For the calculation, the edifice is assumed to be elastic, homogeneous and isotropic, with a Young's modulus of 5 GPa, and a Poisson's ratio of 0.25 (Cayol, 1996). The shape of the structures (topography, dykes and magma chamber) is modelled by meshes with triangular elements. The topography is meshed from a 25 m resolution digital elevation model over an 18 km wide circular area centred on PdF. The meshed topography has been chosen two times larger than the caldera surrounding the summit cone in order to avoid edge effects (Fig. 2a). The mesh is denser close to the eruptive fissures where displacement gradients are larger, and coarser away from the fissures (Fig. 2a). Surface displacements are calculated at the summits of the mesh elements.

In the absence of magma injection in depth during inter-eruptive periods at Piton de La Fournaise (Brenguier et al., 2008; Peltier, 2007), inter-eruptive displacements from the permanent GPS data can be explained by an over/under pressure magma reservoir. We have modelled such a magma body using an ellipsoid shaped over/under pressure source (ΔP). The ellipsoid is defined by the 3D coordinates of its centre and the dimensions of its three half axes (Fig. 2b). Confidence intervals on these parameters are estimated from the one dimensional posterior probability density function (Sambridge, 1999b). On the other hand, syn-eruptive displacements are modelled using dyke-shaped overpressure sources. At PdF, dyke injections propagate first vertically below the Dolomieu crater and then extend laterally (Peltier et al., 2005). Thus, to constrain the vertical and the lateral propagation, the geometry of dykes is defined in two steps (Peltier et al., 2007). The first step is a dyke propagating vertically, modelled from permanent GPS data occurring in the first stage of the magma injection (Table 1), and shaped by six geometrical parameters (3D coordinates of the origin, length, height, and dip; Fig. 2c) and a ΔP. Second, the lateral propagation is modelled from permanent but also reiterated GPS data

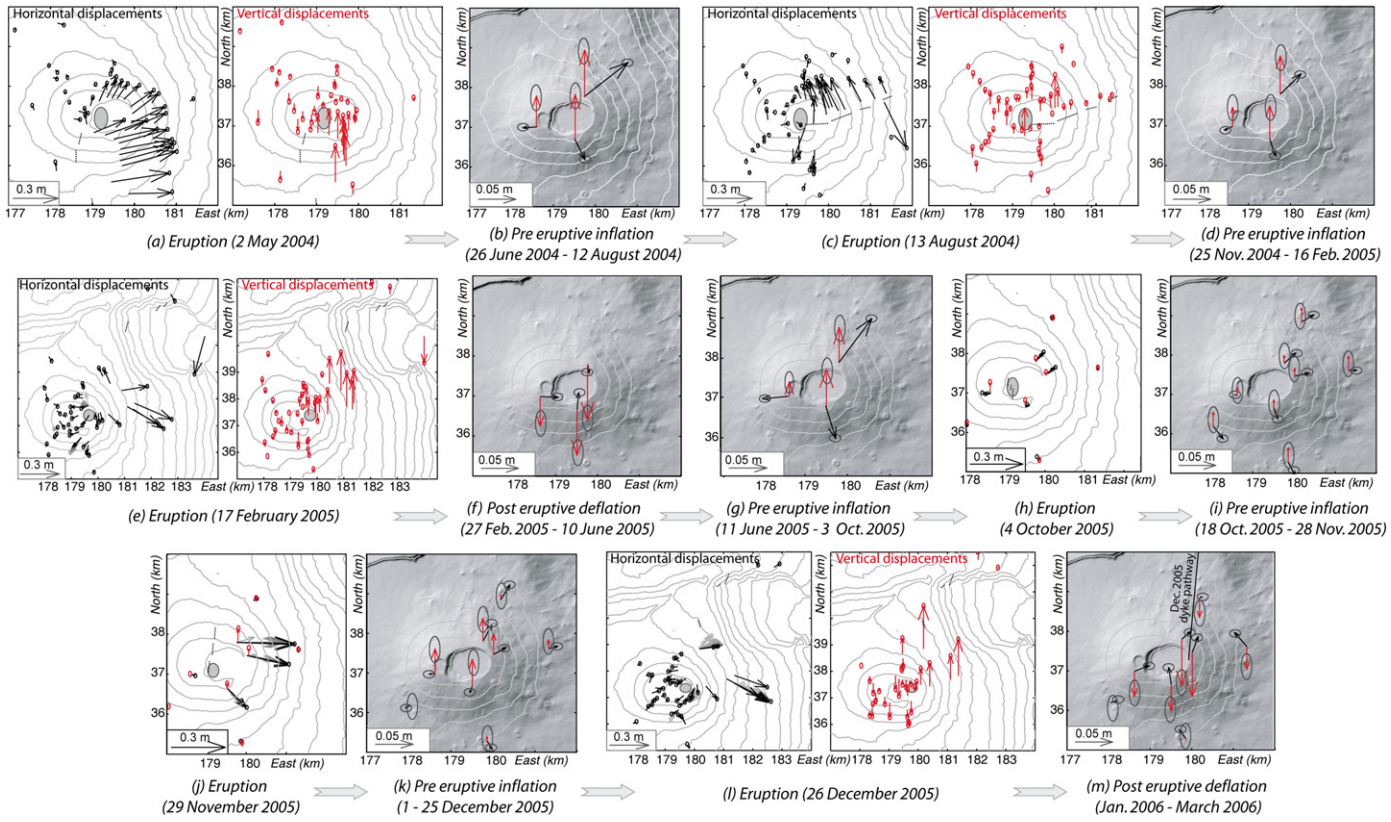

Fig. 3. Displacements monitored by GPS during eruptive (white background) and inter-eruptive (grey background) periods in 2004–2005. Horizontal and vertical displacements are plotted as black and red vectors, respectively. For inter-eruptive periods (b, d, f, g, i, k, m), and for the October and November 2005 eruptions (h, j), only the permanent GPS are available. Reiterated GPS campaigns took place (a) in April and in June 2004, (c) in July and September 2004, (e) in September 2004 and March 2005 (l) in December 2005 and January 2006. Dotted black lines represent the location of eruptive fissures. Grey circles represent the location of the first vertical inflation centre recorded during magma injections (Table 1). (Gauss Laborde Réunion coordinates).

covering the whole magma injection. For the second step, the dyke propagates laterally and is connected to the previous one at an elevation deduced from inversion modelling and connected to the surface at the locations of the eruptive fissures (Fig. 2c). The second stage propagation is defined by a ΔP and six geometrical parameters (dip, elevation of the bottom side, shear – i.e. inclination of the line joining the middle points of the top and bottom sides with the vertical, twist – i.e. angle between the top side and the bottom side, bottom side inclination, and ratio between the length at the top and the bottom of the dyke, Fig. 2c). At PdF, the shape of the dykes observed along the cliffs are never simple, that is why we have chosen to model the dyke propagations with all these parameters, described above and already used at PdF for previous studies (Froger et al., 2004; Fukushima et al., 2005). Previous studies reveal that such a three-dimensional mixed BEM model predicts the geometry at depth better than Okada type models (Fukushima et al., 2005).

2.3. Geochemical analyses

Major and minor elements geochemical analyses were made on glass beads prepared from bulk lava samples, using a Panalytical AXIOS X-ray fluorescence spectrometer at La Réunion University. The spectrometer was calibrated using a set of eight international basic rock standards (NCS standards DC71301, DC72301, DC72302, DC71304, DC73303; CRPG-CNRS standard BE-N and USGS standards BCR-2 and BIR-1). The total error on analyses (due to possible pollutions during bead preparation, to the analytical error of the machine and to the uncertainty on the calibration) was then checked against the BHVO-2 USGS basalt standard and found to lie within the uncertainty of the standard. The total uncertainty on concentration measurements is therefore better than 0.5 wt.% on highly concentrated oxides (typically SiO_2 and Al_2O_3), and about 10 ppm on heavy trace elements (Zr, Ba, Sr, Cr, Co, Ni, Zn).

3. Results

3.1. Ground displacements

Inter-eruptive and syn-eruptive ground displacements are reported on Fig. 3. The time evolution of displacements is also shown on Fig. 4 on the example of SFR0 station. The chronological sequence of displacements may be described as follows:

(1) In pre-eruptive periods, displacements were small (0.3–0.7 mm d^{-1} or 50 mm over 3 months), indicating a slow inflation of the volcano (Figs. 3 and 4a). Displacement vectors were oriented in the same direction from a pre-eruptive inflation to the next (Fig. 3). These displacements were coeval with a progressive increase of the seismicity (Fig. 4b).

(2) 20 to 180 min prior to each eruption, large inflation-related displacements were monitored (up to 19×10^3 mm d^{-1}), accompanied with a significant increase of the seismicity (Figs. 3 and 4a, b). The corresponding displacement vectors were systematically oriented away from the eruptive vents (Fig. 3).

(3) During the May 2004, August 2004, February 2005 and December 2005 events, syn-eruptive summit deflation (up to 2.4 mm d^{-1}) was monitored, whereas no significant deformation was detected during the October and November 2005 eruptions (Table 1, Fig. 4a).

(4) After the two largest effusive events (February 2005 and December 2005, Table 1), post-eruptive summit deflations occurred (0.3–1.3 mm d^{-1}, Figs. 3 and 4a), whereas a new inflation of the summit cone (0.3–0.7 mm d^{-1}) was monitored after the other eruptions (May 2004, August 2004, October 2005 and November 2005), beginning a new pre-eruptive period as in (1). Note that for the post-eruptive deflation occurring after the

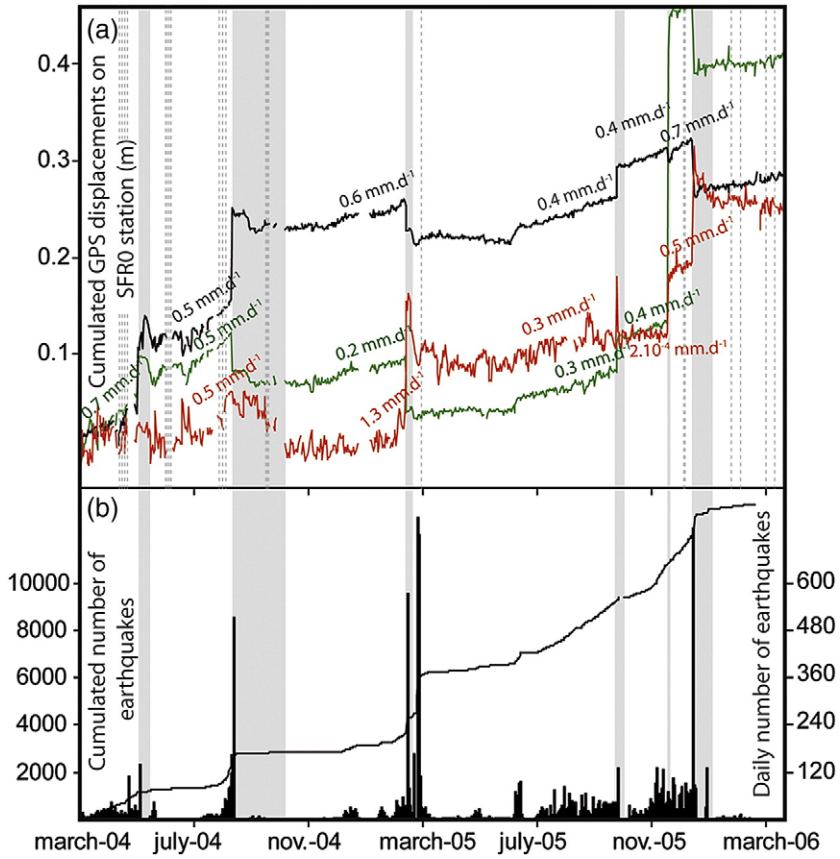

Fig. 4. (a) Cumulated displacements recorded on the SFR0 summit permanent GPS (green: *X* component, black: *Y* component, red: *Z* component). The dotted lines represent dates of the reiterated GPS measurements. (b) Daily (histogram) and cumulated (curve) number of volcano-tectonic earthquakes below the Piton de La Fournaise from March 2004 to February 2006. Shaded areas represent eruptive periods.

December 2005 eruption, a dyke contraction was also recorded by GPS located along the dyke pathway (Fig. 3m).

Overall, the data define two periods of continuous inter-eruptive inflation (February 2004 to February 2005 and June 2005 to December 2005) separated by a three months period of deflation (Fig. 4).

3.2. Modelling of magma bodies

3.2.1. Magma storage zones

Because of the limited number of GPS stations before August 2005, only the pre-eruptive summit inflation preceding the November 2005 and the December 2005 eruptions could be modelled (Fig. 5, Table 1). The horizontal displacements revealed a common behaviour from the two pre-eruptive summit inflations, whereas the vertical displacements differed. The displacement preceding the December 2005 eruption consisted of a generalised uplift at all basal and summit GPS stations (Fig. 3k). This motion can be modelled by an ellipsoidal pressure source located beneath the Dolomieu crater, ~500 m large in diameter (610±170 m on *X* and 480±120 m on *Y*), whose bottom is located at 2260±490 m depth (Fig. 5b). The error on the depth is large due to the GPS error on the *Z* component and the limited amount of data available for the inversion (8 permanent GPS stations). The magma volume variation in the storage zone (ΔV_m) is estimated to reach 0.4×10^6 m^3.

Before the November 2005 eruption, the overall displacement on GPS basal stations was an uplift, whereas the summit stations exhibited purely horizontal and centrifugal displacements (Fig. 3i). In the absence of summit uplift, the motion cannot be modelled by a simple overpressured ellipsoidal source as for December 2005.

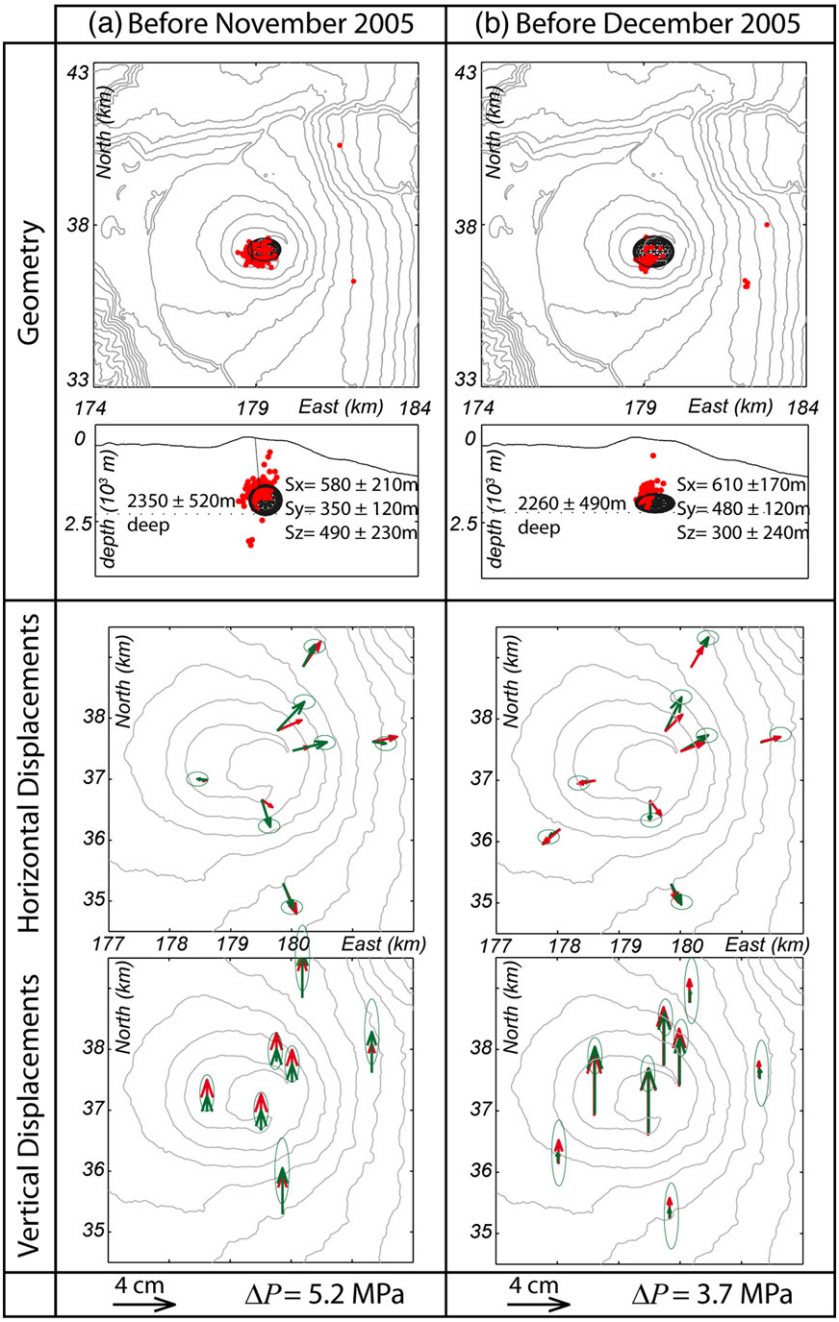

Fig. 5. Geometry of the magma chamber modelled for the (a) November and (b) December 2005 pre-eruptive inflations; together with the location of earthquake hypocenters (red points) related to these pre-eruptive periods. And comparison between observed (green) and calculated displacements (red) (Gauss Laborde Réunion coordinates).

However, it is successfully modelled by an overpressure due to two interconnected magma bodies (Fig. 5a): 1) the dyke emplaced during the October 2005 eruption; 2) an ellipsoidal pressure source located beneath the Dolomieu crater, ~400 m large in diameter (580±210 m on *X* and 350±120 m on *Y*), which bottom is located at 2350±520 m depth. The ΔV_m involved in the overpressure is estimated to reach 0.7×10^6 m^3.

To check if only a single pressure source was involved in the inter-eruptive deformation, we have constrained ΔP which best explained the observed data for the previous pre-eruptive inflations and post-eruptive deflations using the same source as previously found (Fig. 5b). The consistencies of our results are summarized in Table 1. Note that for the post-eruptive deflation following the December 2005 eruption, we have involved both a deflation in the magma reservoir but also a contraction of the December 2005 dyke, previously modelled (Fig. 3m).

3.2.2. Dyke injections

Fig. 6 shows the geometry of dykes that best explains the displacements associated with the six eruptions covering the studied period. Table 1 summarizes the pressures and volumes associated to the modelled dykes.

Dykes feeding the May 2004, August 2004, October 2005 and November 2005 eruptions root below the western part of the Dolomieu crater at depths of 1900–2100 m. These dykes propagate laterally at shallow depths (700–1100 m). On the other hand, dykes feeding the distal eruptions of February 2005 and December 2005 root below the eastern part of the Dolomieu crater at 2150–2450 m depth and propagate laterally toward the lower parts of the edifice. Note that the second part of the February 2005 eruption ("Trou Caron" and "Trou de Sables" vents, location Fig. 1b) was not modelled because of the lack of GPS data in this area. The volume of the magma emplaced during the February 2005 eruption is therefore underestimated.

Syn-eruptive displacements of October and November 2005 are modelled by two injections along one single dyke (Fig. 6). The November 2005 injection followed the same lateral pathway as in October 2005 and propagated further away. The dyke emplaced in October was therefore probably still molten enough to allow the November eruption to take the same pathway.

3.2.3. Causes of uncertainty in the models

Misfits between observed and modelled displacements are reported in Table 1. The precision on GPS data (±0.2 cm on *X* and *Y* component, up to±3 cm on *Z* component) is the main source of error in our models and may cause an uncertainty of ±150 m on depth estimates of the pressure sources (but less than 20 m on *X* and *Y* position), regardless of other uncertainties. In addition, discrepancies between modelled and measured ground displacements can result from the simplifying assumptions made in the models. First, the edifice is considered to be elastic and homogeneous. In reality, the summit cone is fractured and composed of accumulated lava flows, and is thus a non-elastic heterogeneous medium. For instance, the summit and the rift zones are more fractured and are often intruded by dyke injections. The summit and the rift zones are hence possibly characterized by a lower Young modulus than assumed in our models. This heterogeneity in the medium is confirmed by higher seismic velocities below the summit and along the rift zones (Nercessian et al., 1996; Brenguier et al., 2007). Consequently, the assumption of elastic response to the overpressures yields a possible underestimate of the volumes of magma involved in the pressure sources. Another possible limit of our model is that deep pressure sources do not induce ground displacement at the surface of the volcano. In this case also, our model

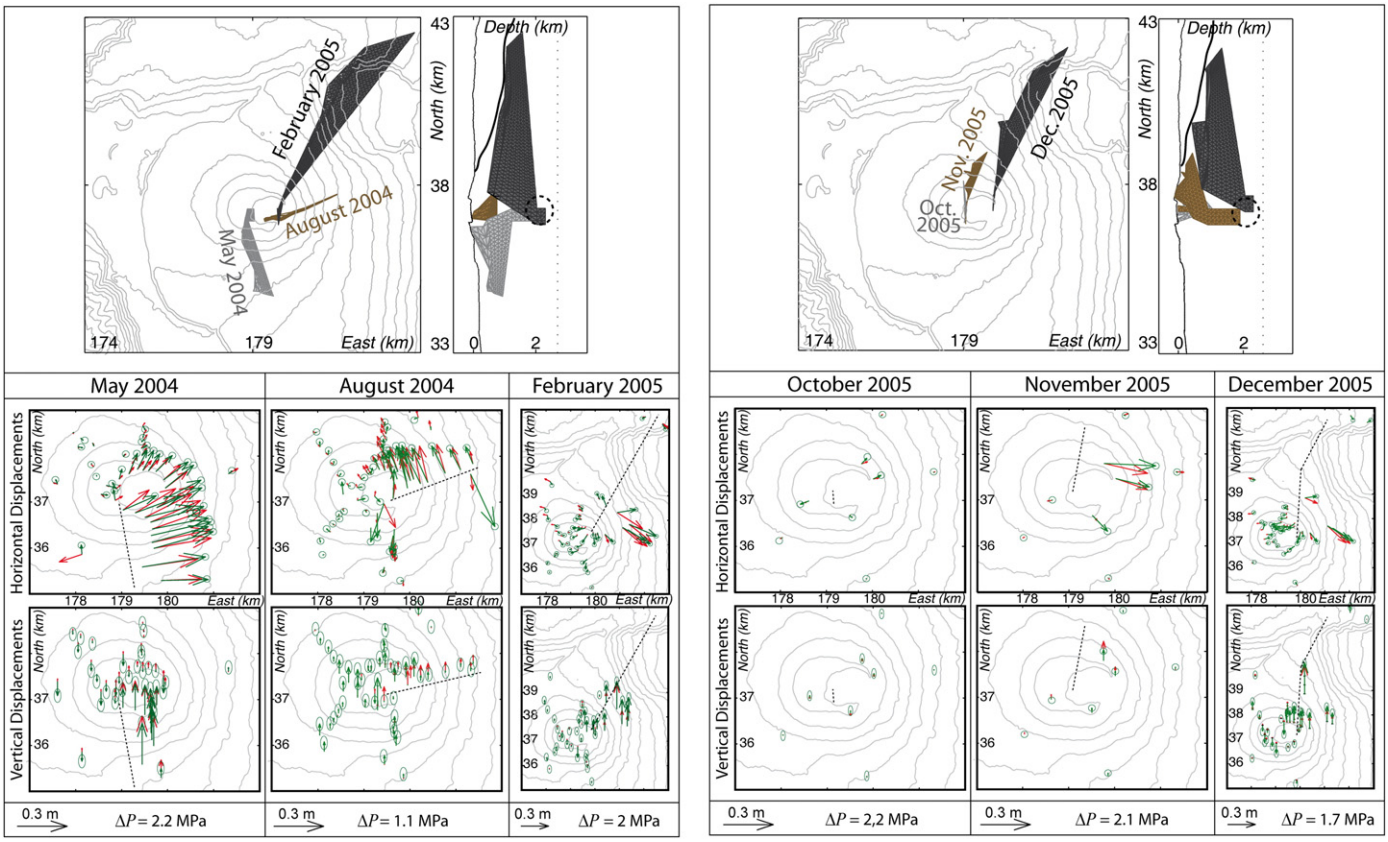

Fig. 6. Geometry of the dykes modelled for the May 2004, August 2004, February 2005, October 2005, November 2005 and December 2005 eruptions. And comparison between observed (green) and calculated displacements (red). Dotted lines represent dyke pathways and dotted circles the location of the magma reservoir previously found (Fig. 5) (Gauss Laborde Réunion coordinates).

may underestimate the volumes of magma involved in the surface deformations. For dyke modelling, misfits can also arise from the incorporation of a part of pre-eruptive inflation and/or post-eruptive deflation into the reiterated GPS measurements (Fig. 4).

3.3. Major element composition of erupted lava

The evolution of lava composition with time is reported in Fig. 7 (full chemical analyses provided as Supplementary Material. Lavas emitted at the beginning of May 2004 eruption are differentiated steady-state basalts (Albarède et al., 1997) devoid of phenocrysts (e.g. 6.7 wt.% MgO; 12.2 wt.% Fe_2O_3; 200 ppm Cr; 50.2 wt.% SiO_2; 3.3 wt.% Na_2O+K_2O; 0.32 wt.% P_2O_5). From the beginning of May 2004 eruption, throughout the August 2004 eruption and up to the beginning of the February 2005 eruption, lavas display a progressive enrichment in compatible elements and a corresponding depletion in incompatible elements (+6.6 wt.% MgO; +1 wt.% Fe_2O_3; +250 ppm Cr; −2.95 wt.% SiO_2, −0.5 wt.% Na_2O+K_2O; −0.3 wt.% P_2O_5). Lavas emitted during the February 2005 eruption are olivine-rich basalts. Throughout the eruption, the lavas become rapidly enriched toward the oceanite pole (up to 40 vol.% olivines at Fo_{84-85}, 23.1 wt.% MgO; 15.4 wt.% Fe_2O_3; 1760 ppm Cr; 43.7 wt.% SiO_2; 2.1 wt.% Na_2O+K_2O; 0.18 wt.% P_2O_5 at the end of the eruption). During the October and November 2005 eruptions, lavas shift back to a steady-state basalt composition, then again evolve rapidly to an oceanite composition during the December 2005 eruption with compositional shifts similar to the May 2004–February 2005 evolution.

4. Discussion

4.1. Magma storage

Contrary to the cycles of inflation/deflation observed at Kilauea volcano between 1970 and 1985 (Yang et al., 1992), no dyke growing occurred during the pre-eruptive inflations at PdF. The pre-eruptive ground deformation can be explained by the inflation of a shallow magma reservoir. A first important result of our modelling is that November and December 2005 pre-eruptive deformations can be explained by a single common source (same depth and same size within the uncertainties), from which dykes are emitted (see consistencies on Table 1, Fig. 6). The magma reservoir predicted by our model is consistent with the presence of a low velocity zone at sea level inferred from seismic waves inversion (Nercessian et al., 1996). In addition, our proposed magma reservoir is located just beneath the pre-eruptive swarm of earthquakes consistently recorded at 500 to 2300 m depth during the August 2004 to December 2005 period (Fig. 5) and during previous eruptions (Battaglia et al., 2005). The seismic swarm represents a highly stressed zone, interpreted as the roof of a magma reservoir (Nercessian et al., 1996), whose location is in agreement with our modelled pressure source. This reservoir is also consistent with, but better constrained than, the pressure source modelled from the August to September 2003 activity (Peltier et al., 2007). A single reservoir may hence be responsible for all the eruptions since 2003.

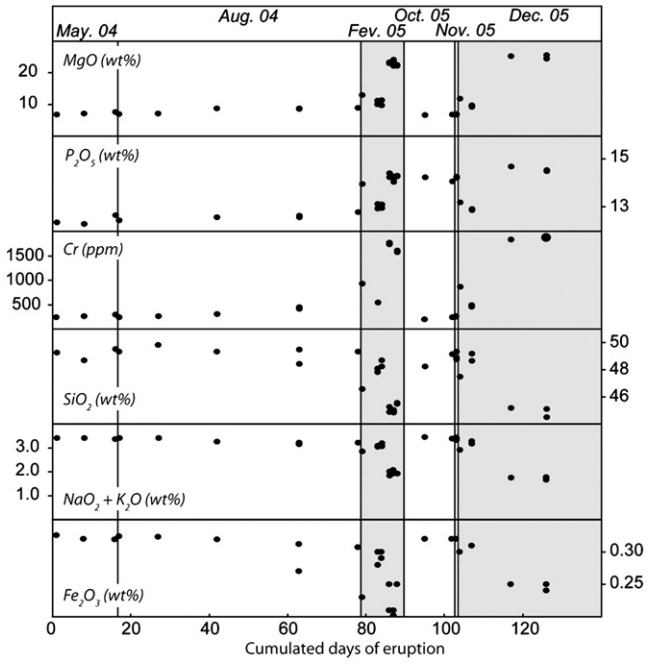

Fig. 7. Composition evolution of lavas with time between May 2004 and January 2006. Shaded areas represent oceanite eruptions.

4.2. Dyke injections

Another important implication of modelling and geochemistry is that two preferential dyke pathways can be distinguished (Figs. 3, 6). Dykes feeding proximal and summit eruptions root at shallow level, beneath the Dolomieu crater or on its western part, and propagate vertically. Lavas emitted during these eruptions are differentiated steady-state basalts. Regarding location, elevation (2300 m±500 m depth) and shape of the modelled magma reservoir (Figs. 5, 6), we suggest that these dykes initiate (1900–2100 m depth) at the top of the magma reservoir where the lava composition is less primitive. On the other hand, dykes feeding the distal eruptions root deeper (2150–2450 m depth) on the eastern part of the Dolomieu crater and propagate laterally on the eastern flank. These dykes transport olivine-rich basalts or oceanites. We suggest that these dykes sample more primitive magmas because they initiate at the base of the reservoir, or from a deeper storage zone. Likely, deeper dykes systematically root and propagate on the eastern side of PdF because the lithostatic load above the base of the reservoir is smaller on the free edge of the edifice. The involvement of olivine phenocrysts in these deeper dykes (olivine-rich basalts and oceanites) increases the viscosity and the density of the magmas. The increase of the density contrast between the magma and the surrounding rocks would avoid a large vertical propagation favouring a lateral propagation toward the flank (Pinel and Jaupart, 2004).

4.3. Eruptive cycles

The two periods of continuous inter-eruptive inflation (February 2004 to February 2005; and June 2005 to December 2005) are coeval with the two periods of compatible element and olivine enrichments in emitted lavas (May 2004 to February 2005 eruptions; and October 2005 to December 2005 eruptions) (Fig. 7). Therefore, deformation and geochemical data define two cycles of volcanic activity. Each cycle begins with a summit inflation that is followed by eruptions of small volumes of differentiated basalt near the summit, fed by dykes initiated at the top of the magma reservoir. The inflation continues until the cycle ends up with lateral eruptions away from the summit, fed by deeper dykes, and emitting large volumes of more primitive, olivine-rich lavas. So during a same cycle, the summit inflates continuously and eruptions occur at lower and lower elevation with increasingly more and more primitive emitted lavas. The two cycles end with a distal eruption draining efficiently the shallow plumbing system with the emission of large volumes of magma (around 20×10^6 m^3), generating then a summit deflation due to mechanical and thermal readjustments of the zone surrounding the feeding pathways (Fig. 3f, m).

This is the first time since the implantation of the volcanological observatory that such quasi-continuous inflation of the summit cone and eruptive cycles are observed. Between 1977 and 2002, only one distal eruption occurred (in 1977) and no significant pre-eruptive

inflation was recorded. The recognition of these volcanic cycles in the recent activity of Piton de La Fournaise suggests that the approximate location of future eruptions might be predicted using deformation data and the geochemistry of the most recent eruptions.

Two end-member scenarios may explain the cyclic deformation and the geochemical pattern of PdF volcano. The first scenario is an open system reservoir, continuously supplied by deeper magmas. In this model, the cyclic inflation of the cone is caused by the refill of the reservoir. At the beginning of the cycle, the volcano is in a state of structural stability because the overpressure is low, and the rupture is favoured at the top of the magma chamber, where the lithostatic pressure is lower (Pinel and Jaupart, 2004; Gudmundsson et al., 2002). Because the volumes emitted during the summit eruptions are small, the pressure continues to increase with increasing magma supply, and causes the destabilization of the free eastern flank of the volcano. In this unstable setting, distal eruptions of magma from flank fissures are facilitated, as suggested for Etna (Allard et al., 2006; Walter et al., 2005) or Kilauea (Owen et al., 2000) volcano. Eventually, the end of the cycle occurs when a flank eruption is large enough to release most of the overpressure and to bring the volcano back to stability for a period of rest. This does not mean, however, an interruption of the deep magma supply to the reservoir. In this scenario, the deflation phase rather occurs because the emission on the flank eruption is larger than the refill flux into the reservoir. The pressure decrease induces readjustments of the edifice around the reservoir, until a cycle starts anew.

The second possible scenario is a closed-system evolution of the magma reservoir, only episodically supplied at brief intervals, such as before the 1998 eruption (Battaglia et al., 2005). In this scenario, the cyclic inflation of the cone is caused by the degassing of the magma batch. Again at the beginning of the cycle, the overpressure is low and produces small summit eruptions of magma sampled at the top, more differentiated part of the reservoir, where the lithostatic pressure is lower. With increasing pressure, the eastern flank of the volcano becomes unstable and allows large lateral eruptions of more primitive magma. These large eruptions release most of the pressure and induce a subsequent period of rest. The next cycle begins after further degassing of the magma batch, or occasionally with a refilling of the reservoir.

In the case of a closed-system reservoir, the volume emplaced as lava flows and dykes (ΔV_e) should be smaller than or equal to the magma volume variation in the storage zone, corrected from decompression (ΔV_{mC}). On the contrary, ΔV_e should be greater than ΔV_{mC} in the case of a refilling of the storage zone during an eruption, or in the case of magmas too deep to induce surface deformation. On Kilauea volcano, magma was estimated to undergo a 400 to 500% expansion during its ascent out of the reservoir (Johnson, 1992). Considering the similarities between Kilauea and PdF volcanoes, it is likely that ΔV_{mC} is 2 to 5 times greater than ΔV_m at PdF. Consequently, ΔV_{mC} should be comprised between 1.4×10^6 m^3 and 3.5×10^6 m^3 for the November 2005 eruption, and between 0.8×10^6 m^3 and 2×10^6 m^3 for the December 2005 eruption. Magma emplaced as dykes and lava flows yielded a ΔV_e of 1.7×10^6 m^3 and 25.2×10^6 m^3 for the November 2005 and December 2005 eruptions, respectively (Table 1). Considering the whole October–November 2005 cycle, $\Delta V_{mC}=3.2$ to 8.2×10^6 m^3 and $V_e=29.3\times10^6$ m^3. Therefore, ΔV_e seems to be 5–10 times greater than ΔV_{mC} for the whole October–December 2005 cycle, i.e. magma emission was too large to explain the observed surface deformations. The same discrepancy is observed for the two pre-eruptive phases modelled for the first cycle (Table 1). A similar case was reported on Krafla volcano (Arnadottir et al., 1998). Deep magma bodies yielding no surface deformation could explain the discrepancy between the emitted volumes and the pre-eruptive deformations. If so, the refill could come from the 7.5 km deep reservoir suggested by Battaglia et al. (2005). The change in the volcano behaviour, with a quasi-continuous inflation during the two eruptive cycles and the succession of numerous eruptions is in agreement with such a quasi-continuous deep refilling.

5. Conclusion

The combination of deformation data, numerical modelling and lava geochemistry on Piton de la Fournaise volcano (La Réunion hotspot) leads us to the following conclusions: 1) The volcanic eruptions of the 2004–2005 period may be explained by a single common magma reservoir, ~500 m large, located at about 2300 m depth. 2) Two cycles of continuous volcano pre-eruptive inflation and compatible element enrichment are evidenced for the May 2004–December 2005 period, with a rest from March to October 2005. 3) At the beginning of each cycle, dykes propagate from the roof of the reservoir and yield eruptions near the summit. At the end of the cycle, dykes propagate from the eastern sidewall of the reservoir and yield lateral eruptions away from the summit. 4) The volumes of magma emplaced during these eruptions appear too large to explain the observed surface deformations and therefore suggest some refill of the reservoir by deeper magmas. These results provide a quantitative basis to predict the location of future eruptions, depending on their timing within a cycle of volcanic activity.

Acknowledgement

We are grateful to Philippe Kowalski and Frédéric Lauret for their help in implementing the GPS network, and to Patrice Boissier for his code allowing data processing. Valérie Ferrazzini is also acknowledged for providing seismic data. We thank V. Pinel for helpful review comments. This is IPGP contribution number 2360.

Appendix A. Supplementary data

Supplementary data associated with this article can be found, in the online version, at doi:10.1016/j.epsl.2008.02.042.

References

Albarède, F., Luais, B., Fitton, G., Semet, M., Kaminski, E., Upton, B.G.J., Bachèlery, P., Cheminée, J.L., 1997. The geochemical regimes of Piton de La Fournaise volcano (Reunion) during the last 530000 years. J. Petrol. 38, 171–201.

Allard, P., Behncke, B., D'Amico, S., Neri, M., Gambino, S., 2006. Mount Etna 1993–2005: anatomy of an evolving eruptive cycle. Earth Sci. Rev. 78, 85–114.

Arnadottir, T., Sigmundsson, F., Delaney, P.T., 1998. Sources of crustal deformation associated with the Krafla, Iceland, eruption of September 1984. Geophys. Res. Lett. 25, 1043–1046.

Bachèlery, P., Mairine, P., 1990. Evolution volcano—structurale du Piton de La Fournaise depuis 0.53 Ma. In: Lénat, J.-F. (Ed.), Le Volcanisme de La Réunion. Centre de Recherches Volcanologiques, Clermont-Ferrand, pp. 213–242.

Battaglia, J., Ferrazzini, V., Staudacher, T., Aki, K., Cheminée, J.L., 2005. Pre-eruptive migration of earthquakes at the Piton de La Fournaise volcano (Réunion Island). Geophysical Journal International 161, 549–558.

Brenguier, F., Shapiro, N.M., Campillo, M., Nercessian, A., Ferrazzini, V., 2007. 3-D surface wave tomography of the Piton de la Fournaise volcano using seismic noise correlations. Geophys. Res. Lett. 34, L02305. doi:10.1029/2006GL028586.

Brenguier, F., Shapiro, N.M., Campillo, M., Ferrazzini, V., Duputel, Z., Coutant, O., Nercessian, A., 2008. Towards forecasting volcanic eruptions using seismic noise. Nat. Geosci. doi:10.1038/ngeo104.

Cayol, V., 1996. Analyse élastostatique tridimensionnelle du champ de déformations des édifices volcaniques par éléments frontières mixtes, Doctorat, Université de Paris VII.

Cayol, V., Cornet, F.H., 1997. 3D mixed boundary elements for elastostatic deformation field analysis. Int. J. Rock Mech. Min. Sci. 34, 275–287.

Froger, J.L., Fukushima, Y., Briole, P., Staudacher, T., Souriot, T., Villeneuve, N., 2004. The deformation field of the August 2003 eruption at Piton de La Fournaise, Reunion Island, mapped by ASAR interferometry. Geophysical Research Letters 31. doi:10.1029/2004GL020479.

Fukushima, Y., Cayol, V., Durand, P., 2005. Finding realistic dike models from interferometric synthetic aperture radar data: the February 2000 eruption at Piton de La Fournaise. J. Geophys. Res. 110. doi:10.1029/2004JB003268.

Gudmundsson, A., Fjeldskaar, I., Brenner, S.L., 2002. Propagation pathways and fluid transport of hydrofractures in jointed and layered rocks in geothermal fields. J. Volcanol. Geother. Res. 116, 257–278.

Johnson, D.J., 1992. Dynamics of magma storage in the summit reservoir of Kilauea volcano, Hawaii. J. Geophys. Res. 97, 1807–1820.

Michon, L., Saint-Ange, F., Bachèlery, P., Villeneuve, N., Staudacher, T., 2007. Role of the structural inheritance of the oceanic lithosphere in the magmato-tectonic evolution of Piton de la Fournaise volcano (La Réunion Island). J. Geophys. Res. 112. doi:10.1029/2006JB004598.

Nercessian, A., Hirn, A., Lépine, J.C., Sapin, M., 1996. Internal structure of Piton de la Fournaise volcano from seismic wave propagation and earthquake distribution. J. Volcanol. Geother. Res. 70, 123–143.

Owen, S., Segall, P., Lisowski, M., Miklius, A., Murray, M., Bevis, M., Foster, J., 2000. January 30, 1997 eruptive event on Kilauea volcano, Hawaii, as monitored by continuous GPS. Geophys. Res. Lett. 27, 2757–2760.

Peltier, A., 2007. Suivi, Modélisation et Evolution des processus d'injections magmatiques au Piton de La Fournaise, Doctorat, Université de La Réunion.

Peltier, A., Ferrazzini, V., Staudacher, T., Bachèlery, P., 2005. Imaging the dynamics of dyke propagation prior to the 2000–2003 flank eruptions at Piton de La Fournaise, Reunion Island. Geophys. Res. Lett. 32. doi:10.1029/2005GL023720.

Peltier, A., Staudacher, T., Bachèlery, P., 2007. Constraints on magma transfers and structures involved in the 2003 activity at Piton de La Fournaise from displacement data. J. Geophys. Res. 112. doi:10.1029/2006JB004379.

Pinel, V., Jaupart, C., 2004. Magma storage and horizontal dyke injection beneath a volcanic edifice. Earth Planet. Sci. Lett. 221, 245–262.

Sambridge, M., 1999a. Geophysical inversion with a neighbourhood algorithm — I. Searching a parameter space. Geophys. J. Int. 138, 479–494.

Sambridge, M., 1999b. Geophysical inversion with a neighbourhood algorithm — II. Appraising the ensemble. Geophys. J. Int. 138, 727–746.

Walter, T.R., Acocella, V., Neri, M., Amelung, F., 2005. Feedback processes between magmatic events and flank movement at Mount Etna (Italy) during the 2002–2003 eruption. J. Geophys. Res. 110. doi:10.1029/2005JB003688.

Yang, X., Davis, P.M., Delaney, P.T., Okamura, A.T., 1992. Geodetic analysis of dike intrusion and motion of the magma reservoir beneath the summit of Kilauea volcano, Hawaii: 1970–1985. J. Geophys. Res. 97, 3305–3324.